Available online at www.sciencedirect.com
ScienceDirect
Ceramics International 34 (2008) 2107–2116
CERAMICS INTERNATIONAL
www.elsevier.com/locate/ceramint

Changes in microstructure of a high chromia refractory due to interaction with infiltrating coal slag in a slagging gasifier environment

Han Bom Kim, Myongsook S. Oh *

Hongik University, School of Chemical Engineering and Materials Science, 72-1 Sangsudong, Mapogu, Seoul, Republic of Korea

Received 31 August 2006; received in revised form 23 April 2007; accepted 14 August 2007
Available online 25 September 2007

Abstract

The changes in microstructures of a high chromia refractory containing Al_2O_3 and ZrO_2 due to interaction with penetrating coal slag under slagging gasifier conditions were investigated. The unused chromia refractory was an inhomogeneous mixture of microstructures of varying shape, size, composition and degree of densification. The chemical structures of Cr were Cr_2O_3 and $(Cr,Al)_2O_3$; of Zr were ZrO_2 and Zr-silicate; of Si were silicates of Al_2O_3 and ZrO_2; and of Al were Al-silicate and $(Cr,Al)_2O_3$. As coal slag infiltrated a chromia refractory, FeO in the slag first reacted with Cr_2O_3 forming $FeCr_2O_4$ until there was no FeO remaining in the penetrating slag. Then, Al_2O_3 in the slag interacted with Cr_2O_3, forming $(Al,Cr)_2O_3$ from the outer edges of the particle. The slag resistance of Cr_2O_3 varied with the particle size and the extent of densification, and the higher resistance was observed in the larger and more densified particles. There was no chemical change in ZrO_2, but it may have dissolved in the slag. The same interaction products were observed in both laboratory-tested and spent refractories from a pilot scale gasifier. The composition and the crystalline phase analyses also support chromite formation at the interface and subsequent depletion of Fe. When the temperature and time were varied, the percent of slag penetrated increased with the exposure time and temperature, though changes in microstructures were difficult to quantify.

Keywords: Gasification process; Chromia refractory; Interaction; Coal slag

1. Introduction

The gasification process converts carbonaceous materials such as coal, petroleum coke, and biomass to synthesis gas, consisting of H_2 and CO that can be utilized as chemical feedstock or for power generation. For gasification of coal and petroleum coke, the most widely used gasifier is the entrained flow type, which operates at high temperature and pressure. Under such conditions, over 99% (with recycling) of the organic portion in the feed is converted to the synthesis gas, while the ash forms a molten slag which flows down the refractory lined wall. Once the slag begins to flow down the refractory wall, the slag penetrates into the porous refractory matrix, and subsequent corrosive reactions occur [1]. Slag penetration and chemical corrosion are the primary causes for refractory degradation in a gasifier [2], and affect the refractory lifetime as well as the economics of the gasification process.

Chromia or chromia–alumina refractory have been used to line gasifiers because of the low solubility of chromia in slag, and zirconia is often added because it improves thermal shock resistance. When alumina and zirconia are added to the chromia, the resulting refractory brick contains various microstructures, and each microstructure reacts differently with the penetrating slag. The penetrating slag composition also changes due to the reaction with the refractory components.

This work investigates changes in microstructures of a high chromia refractory containing alumina and zirconia due to interaction with the penetrating slag. Unused and exposed refractory bricks both from laboratory tests and from a pilot scale gasifier after 1000 h of operation were analyzed for composition, crystalline phase, and microstructures. The microstructures and composition of used refractory materials were evaluated as a function of the slag penetration depth. The effects of exposure temperature and time were also investigated.

* Corresponding author. Tel.: +82 2 320 1480; fax: +82 2 3143 0880.
E-mail address: msoh@hongik.ac.kr (M.S. Oh).

0272-8842/$34.00
doi:10.1016/j.ceramint.2007.08.010

2. Experimental procedure

The laboratory experiments were carried out according to the KS L 3130, Testing Method for Slag Corrosion of Refractories using Crucibles [3]. Crucibles were molded from refractory powders using 10% water. The crucibles were then dried at 30 °C and cured at 1200 °C. For coal ash, Datong coal, a bituminous coal from Datong, China, was ashed at 700 °C. The compositions of Datong coal ash and refractory are listed in Table 1. The shape and dimensions of the refractory crucible are shown in Fig. 1.

The refractory crucible was placed in a constant temperature zone of a tube furnace, and was heated in air at 10 °C/min to 1000 °C, then at 5 °C/min to the testing temperature. When the testing temperature was reached, a 20/80 mix of CO/CO_2 gas was injected at 1000 cm^3/min to simulate a reducing environment. A total of 30–50 g of Datong coal ash was added slowly into the crucible, making sure that the slag was completely melted before the next addition. Slag additions usually took 2–2.5 h. Corrosion tests were carried out at temperatures ranging from 1400 to 1600 °C for 1–6 h, excluding the slag feeding time. Upon the completion of the test, the slag containing crucible was cooled at 2 °C/min to 1200 °C, then the power to the furnace was turned off, allowing the sample to be cooled by natural convection. The exposed crucible was cut along the center axis, and the physical appearance of the remaining slag and refractory, the crack formation, and the percent slag penetrated were recorded.

The spent refractory liners evaluated in this paper were obtained from a 3 tonnes/day pilot scale gasifier at the Institute of Advanced Engineering (IAE), Suwon, Korea. The schematic of the IEA gasifier refractory structure is shown in Fig. 2. The refractory was air cooled, and removed after 1000 h of operation. The gasifier had four feed nozzles, labeled as A, B, C, and D, arranged at 90°. Six liner samples were taken from the following locations: one each from the location at 50 cm below Nozzle A, 40 cm below Nozzle B, 35, 40, and 50 cm below Nozzle D, and one from the slag tap. Each sample was cut into 1 cm sections from the slag face to the outer direction radially, and marked according to the location and depth from the slag face. For example A50-1 is the sample from 50 cm below Nozzle A to a depth 1 cm from the slag face, and D40-10 is the sample from 40 cm below Nozzle D to a depth 9–10 cm from the slag face. Each section was analyzed for chemical composition by X-ray fluorescence (XRF) and crystalline phase by X-ray diffraction (XRD). The changes in microstructure were investigated using a scanning electron microscope with an energy dispersive X-ray attachment (SEM EDX, Hitachi S-2500).

Table 1
Normalized composition of coal ash and a high chromia refractory (wt.%)

	Datong ash	Chromia refractory
SiO_2	55.2	8.3
Al_2O_3	19.0	24.6
Fe_2O_3	15.4	0.7
CaO	6.2	1.8
Cr_2O_3	–	52.7
ZrO_2	–	9.4
MgO	1.0	0.4
MnO	0.3	–
Na_2O	0.5	1.0
K_2O	1.4	–
TiO_2	0.8	1.8
P_2O_5	0.2	–
SUM	100	99.9

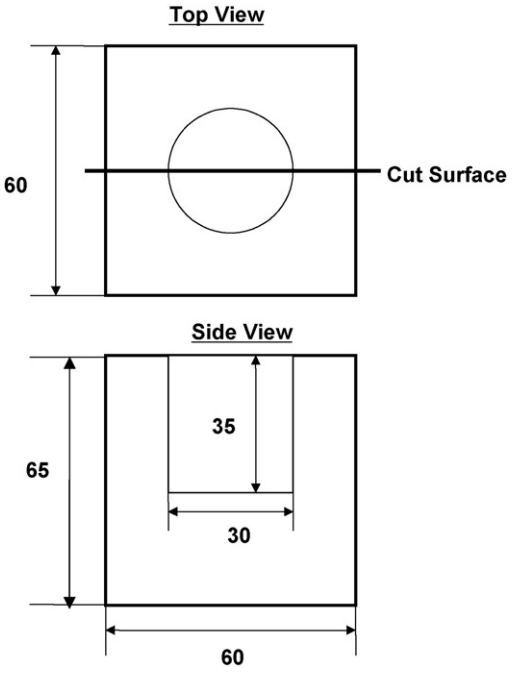

Fig. 1. Crucible size (mm) and sample cutting direction.

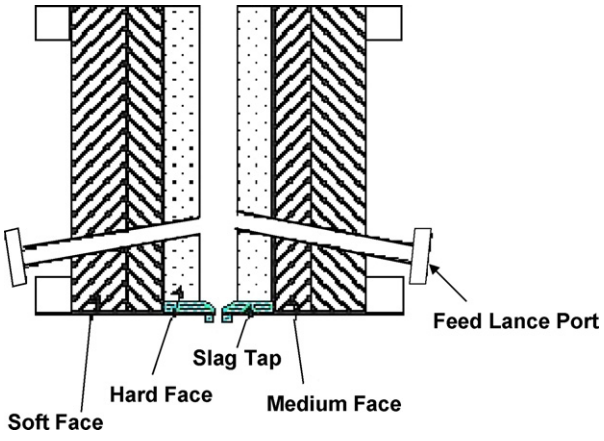

Fig. 2. Refractory structure of the 3 tonnes/day IAE gasifier.

3. Results and discussion

3.1. Microstructures in the unused refractory

Microstructures existing before corrosion by the coal slag were evaluated. Several points in the unused brick were analyzed, and the representative micrographs are shown in Fig. 3. Fig. 3(a) shows an area 1 mm from the surface consisting

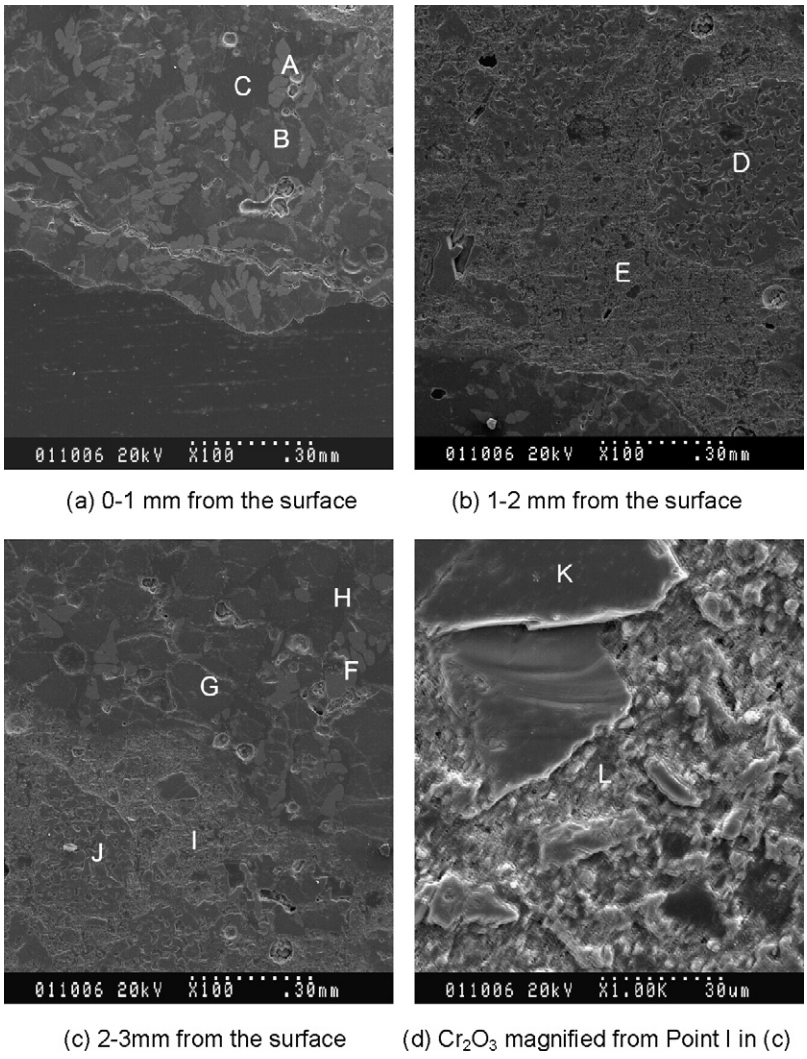

Fig. 3. SEM micrographs of unused chromia refractory brick at different locations in the refractory: (a) 0–1 mm, (b) 1–2 mm, and (c) 2–3 mm from the surface; (d) Cr_2O_3 magnified from Point I in (c).

of light-grey phases (Point A) with a smooth curved boundary and scattered dark-grey phases (B) on a darker background (C). The point composition analyses by SEM EDX showed that the light-grey phase (A) was ZrO_2, the dark-grey phase (B) consisted of 60% Cr_2O_3 and 18% Al_2O_3, and the darker background was 49% SiO_2, 29% ZrO_2, and 13% Al_2O_3. Fig. 3(b) shows a region 1–2 mm below the surface and consists of densified Cr_2O_3 (D) as well as a porous area (E) containing small particles of Cr_2O_3. The two main components of the area shown in Fig. 3(b) were Cr_2O_3 (75%) and Al_2O_3 (12%), and the concentrations of SiO_2 and ZrO_2 were 3 and 6%, respectively. Fig. 3(c) is 2–3 mm from the surface and consists of five different phases. On the top of the micrograph, grey ZrO_2 (F), dark $Cr_2O_3 + Al_2O_3$ (G), and a darker background of $SiO_2 + Al_2O_3 + ZrO_2$ (H) were observed. At the bottom, small particles of Cr_2O_3 in the porous area (I), and densified Cr_2O_3 (J) were observed. Fig. 3(d) magnifies Point I in (c), and presents a clear picture of large particles of Cr_2O_3 (K) and surrounding small Cr_2O_3 particles (L). The region between 3 and 4 mm from the surface was similar to Fig. 3(a), and the 5–6 mm region showed many small particles of ZrO_2.

As shown, the unused chromia refractory was a heterogeneous mixture of microstructures varying in shape, size, composition and degree of densification. The chemical structures of each major element were as follows: Cr existed as Cr_2O_3 or $(Cr,Al)_2O_3$, Zr as ZrO_2 or Zr-silicates, Si as silicates of Al_2O_3 and ZrO_2, and Al as aluminasilicate or $(Cr,Al)_2O_3$. However, the only phases confirmed by XRD were eskolaite (Cr_2O_3) and ZrO_2, as shown later in Fig. 10. XRD analysis gives only the major phases, and not all microphases observed using SEM were identified by XRD.

3.2. Changes in microphase in the laboratory-tested bricks

The slag/refractory microstructures as a function of infiltrating depth are shown in Figs. 4 and 5 for samples tested at 1500 °C for 4 h using Datong coal ash. Fig. 4(a)–(c) shows the slag area, which contains a dispersed crystalline phase. Area A in Fig. 4(a) is magnified in (b) and shows a dendritic phase, probably formed during cooling of the ash. Area B in Fig. 4(a), magnified in (c), shows a particle phase consisting of mainly Cr and Fe with a small amount of Al. The

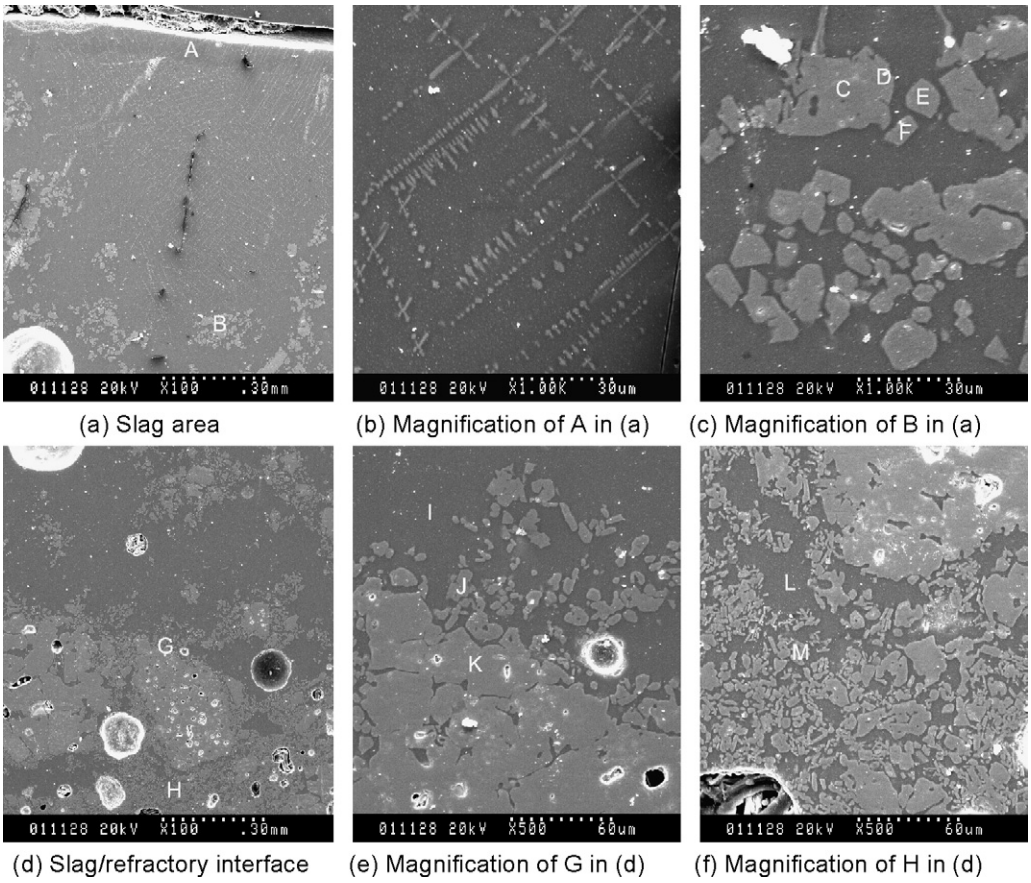

Fig. 4. SEM micrographs of the slag/refractory interface after exposure to slag at 1500 °C for 4 h under a 20/80 mix of CO/CO_2 atmosphere: (a) slag area, (b) magnification of A in (a), (c) magnification of B in (a), (d) slag/refractory interface, (e) magnification of G in (d), and (f) magnification of H in (d).

point composition was taken from four locations, marked as D through F in Fig. 4(c). On an oxide basis, Point C had 76% Cr_2O_3 and 23% Fe_2O_3; D, 62% Cr_2O_3 and 25% Fe_2O_3; E, 23% Cr_2O_3 and 65% Fe_2O_3; and F, similar to E. The Cr concentration was higher in large fragments than in small fragments, and present at higher concentrations at the center than at the edges. The Fe concentration in these products was higher in the small fragments and at the edges of large fragments. The Cr–Fe particles dispersed in slag showed more angled boundaries than those found in the refractory, suggesting that Cr_2O_3 first dissolves in the slag, forms $(Fe,Cr)_3O_4$ which probably precipitates out during the cooling.

Fig. 4(d)–(f) shows micrographs at the slag/refractory interface. Areas G and H in Fig. 4(d) are magnified and shown in (e) and (f), respectively. Fig. 4(e) shows a clear boundary of the slag and the refractory. The slag phase (I) consists of Ca–Al–Si oxides with about 8% FeO and a dispersed phase (J) of Cr–Fe–oxide with a higher concentration of Fe than Cr (29%

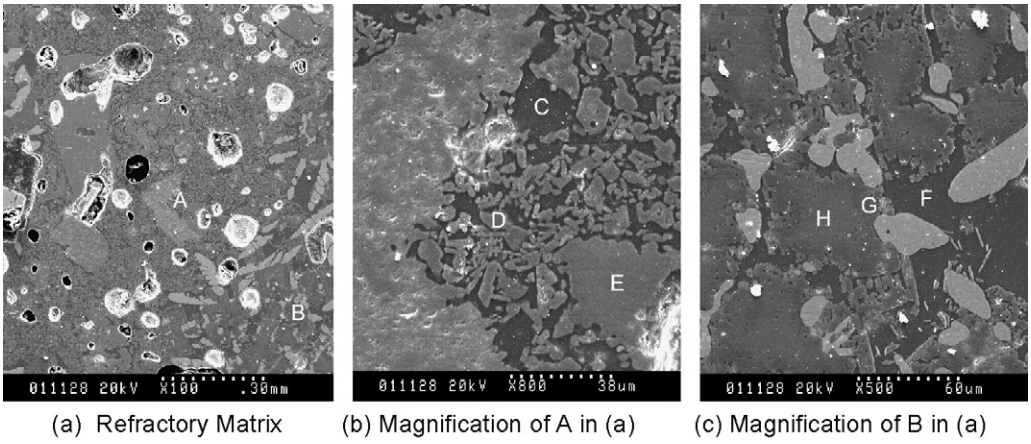

Fig. 5. SEM micrographs of the area 1 mm from the slag/refractory interface after exposure to slag at 1500 °C for 4 h under a 20/80 mix of CO/CO_2 atmosphere: (a) refractory matrix, (b) magnification of A in (a), and (c) magnification of B in (a).

Cr_2O_3; 57% Fe_2O_3) and the surface of the refractory shows a continuous layer (K) of Cr–Fe–oxide with the higher concentration of Cr than Fe (58% Cr_2O_3, 31% Fe_2O_3). Fig. 4(f) is an area about 0.3 mm below (e), and contains severely fragmented particles. Area L in Fig. 4(f) shows the infiltrated slag phase, while small fragments (M) are Cr–Fe–Al oxide with 59% Cr_2O_3, 17% Al_2O_3 and 15% Fe_2O_3, on an oxide basis. Even though Fig. 4(f) was taken from a region 0.3 mm below (e) micrograph, the slag phase and the fragment particles contained lower Fe concentrations than those in (e).

In light of the XRD analyses explained in Section 3.4, the Cr–Fe–Al oxide at the interface has the crystalline structure of ironchromites ($FeCr_2O_4$) in the spinel group, despite the varying ratio of Fe to Cr. Therefore, the dominant reaction product at the slag/refractory interface can be expressed as $(Fe,Cr)_3O_4$, and is probably formed from the reaction between FeO in the slag and Cr_2O_3 in the refractory under reducing conditions. All other tested bricks consistently showed $(Fe,Cr)_3O_4$ formation at the slag/refractory interface.

The degradation of the inside refractory matrix by infiltrated slag is shown in Fig. 5(a), which covers the area 1.1 mm below the area shown in Fig. 4(d). The center and the upper left side of Fig. 5(a) shows both the large particles and fragments (area A), while the lower right side shows a grey phase with curved boundaries and dark particles (area B). The round, white spots as well as the dark-black holes are pores. When area A is magnified 800-fold (Fig. 5(b)), one can observe that the densified large Cr_2O_3 on the left side was little affected except on its jagged edges. The various size fragments (D and E) were both $(Cr,Al)_2O_3$ and the background (C) is the slag phase, consisting of SiO_2, Al_2O_3, CaO, and a low level of FeO. Fig. 5(c) magnifies area B in (a), and shows light-grey ZrO_2, and $(Cr,Al)_2O_3$ particles with jagged edges. It was noted that the edges of several $(Cr,Al)_2O_3$ particles have a darker grey color than the center. The point composition analyses at G and H in Fig. 4(c) shows that the dark edge contains 53% Cr_2O_3 and 42% Al_2O_3, while the lighter center contains 82% Cr_2O_3 and 16% Al_2O_3, confirming that the dark-grey edge was rich in Al_2O_3, and that the concentration of Al_2O_3 decreased as the grey became lighter towards the center.

The fact that very little Fe was detected in this area suggests that Fe in the slag was depleted at the slag/refractory interface, forming $(Cr,Al)_3O_4$. From the Al-rich edges and fragments of Al-rich $(Cr,Al)_2O_3$, it was concluded that once Fe was depleted, Al_2O_3 in the slag interacted with Cr_2O_3 or $(Cr,Al)_2O_3$ and formed the Al_2O_3-rich edges or Al-rich $(Cr,Al)_2O_3$. The well-densified large Cr_2O_3 grains were less affected than the small particles.

Compared to Cr_2O_3 and $(Cr,Al)_2O_3$, ZrO_2 does not seem to be greatly affected by slag. There was no evidence of a chemical reaction between ZrO_2 and infiltrated slag. Even the physical structure did not appear to change greatly with ZrO_2 maintaining a smooth grain boundary as shown in Fig. 3(a). However, the point composition of the infiltrated slag consistently showed the ZrO_2 concentration at 7–11% level, indicating the possibility of ZrO_2 dissolution in the slag.

3.2.1. Effect of temperature

The effect of temperature was investigated at 1400, 1500 and 1600 °C using 50 g of Datong ash. The ash feeding time varied because of the difficulty in melting ash at 1400 °C and because of bubbling at the higher temperatures. The total feeding time was 2.5 h at 1400 °C and 2 h at 1500 and 1600 °C.

The amount that the slag penetrated increased as the temperature increased because of the lower viscosity at higher temperature. The amount of slag infiltrated into the refractory was determined from the height of the slag remaining in the cup after the test. As shown in Table 2, 14% of the slag infiltrated into the refractory matrix at 1400 °C, while 29 and 64% infiltrated at 1500 and 1600 °C, respectively. The viscosity was measured using a Searle-type coaxial cylindrical viscometer, as the slag was cooled at 2 °C/min. The viscosity of Datong ash was 520 P at 1400 °C, 227 P at 1500 °C, and less than 190 P at 1600 °C.

The micrographs after 4 h of corrosion (excluding feeding time) at each temperature are compared in Fig. 6. Fig. 6(a)–(c) shows the slag/refractory interface: a clear boundary was observed at 1400 °C, while it was difficult to distinguish the boundary at 1600 °C. At all temperatures, the interface reaction product was chromite. As was the case at 1500 °C (Fig. 4), a variation in Fe concentration was observed at other temperatures: the Fe concentration was higher in the small size chromite dispersed in the slag than in larger aggregated chromites, and the Fe concentration at the edges of the large particles was higher than the concentration in the center.

It was difficult to compare the severity of degradation as a function of temperature inside the refractory matrix because of the inhomogeneity of the refractory brick. Representative micrographs near the interface at each temperature are shown in Fig. 6(d)–(f). At 1400 °C, the short rod-shaped $(Cr,Al)_2O_3$ particles appear as aggregates. The fragment particles appear to become more dispersed as the temperature increases, indicating more corrosive degradation at higher temperatures.

3.2.2. Effects of exposure time

The effect of exposure time was investigated by varying the holding time at 1600 °C from 1 to 6 h, excluding 2 h of slag feeding time. It was difficult to make even a qualitative comparison of microstructures near the interface, so only the degree of slag penetration was compared. Table 2 compares the percent slag penetration, showing an increase with time. After 6 h at 1600 °C, nearly the entire slag penetrated into the refractory.

Table 2
Effect of temperature and holding time on slag penetration

Temperature (°C)	Holding time (h)	Viscosity (P)	Slag penetrated (vol.%)
1400	4	520	14
1500	4	227	29
1600	4	<190	64
1600	1	<190	45
1600	2	<190	63
1600	6	<190	94

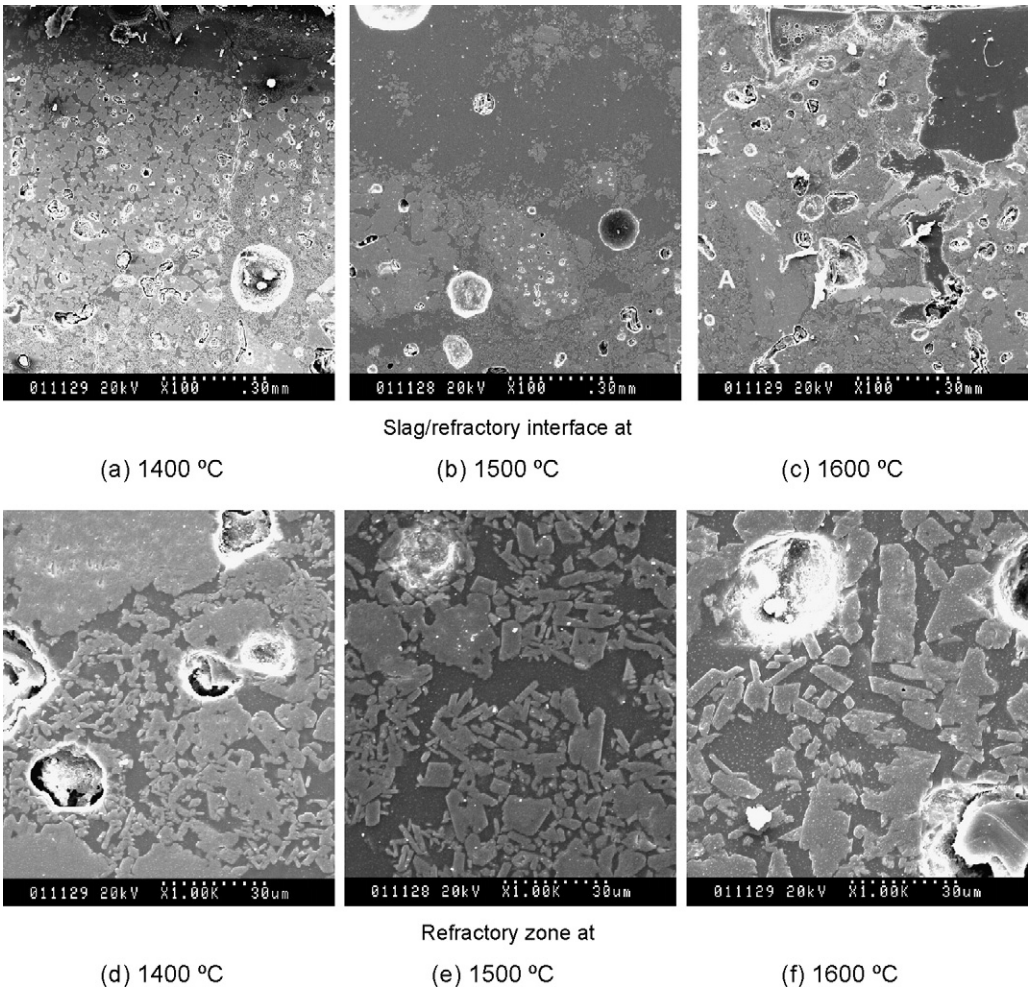

Fig. 6. SEM micrographs after 1400, 1500, 1600 °C slag exposure under a 20/80 mix of CO/CO_2 atmosphere: (a)–(c) slag/refractory interface and (d)–(f) refractory zone.

3.3. Interaction products in the spent refractory liners from a pilot scale gasifier

The slag/refractory interface in the spent refractory liner was investigated using D35, A50 and slag tap samples. These samples had a relatively thick slag layer remaining on the brick, which contained a high concentration of chromite. These samples also had a thick chromite layer on the refractory side, which could be observed easily, even at 100-fold magnification.

Fig. 7(a) and (b) are micrographs of D35. Fig. 7(a) shows the area with dispersed crystalline phases (A) and the area packed with the same phase (B). The dark background in A is the slag phase containing Ca–Al–Si oxides, and the crystalline phases in both A and B are chromites. Fig. 7(b) magnifies area A in (a), and shows $(Fe,Cr)_3O_4$ with clear angled boundaries on the glassy silicate phase. The needle shaped phase in the slag had a composition of Si–Fe–Al, but the XRD analysis did not identify any relevant crystalline phase. Fig. 7(c) and (d) are from slag tap sample. Fig. 7(c) can be divided into three regions: Cr-rich $(Fe,Cr)_3O_4$ area, Fe-rich $(Fe,Cr)_3O_4$, and Ca–Al–Si slag phase. Fig. 7(d) magnifies area C in (c), and shows the same chromite phase (D) as seen in Fig. 7(b). Fig. 7(e) and (f) are micrographs of A50. Fig. 7(e) shows a continuous layer of chromite at E, and dispersed chromites in the slag at F. Fig. 7(f) magnifies (e)-E, and shows an even denser layer of chromite than the slag tap sample shown in Fig. 7(d).

The interaction of the inner layer with the Fe-depleted slag was similar to what we observed in the laboratory sample. Fig. 8 shows the micrographs of B40-1, which is the first 10 mm from the slag face, and is the area affected by the slag. The total penetration depth of B40 was about 20 mm [4].

Fig. 8(a) shows the region 5–6 mm from the slag face, and contains dark Cr_2O_3–Al_2O_3 phase (A) around a pore, which appears as a bright circular shape, and well-densified Cr_2O_3 phase (B). Fig. 8(b) is a magnified micrograph of area A in (b), and Fig. 8(c) that of area B in (b). Fig. 8(b) shows fragments of the Cr_2O_3–Al_2O_3 phase around relatively large particles with dark-grey edge, rich in Al_2O_3. The well-sintered Cr_2O_3 in Fig. 8(c) did not show much change in the particle structure, though small pores were observed on the surface. Comparison with the large densified grains of Cr_2O_3 in unused sample (Fig. 3(b)) led us to believe that these small pores in Fig. 8(c) were formed due to the exposure to slag, unlike the large pore shown in Fig. 8(a) which was probably formed during the curing stage. Therefore, the spent refractory also shows the interaction of refractory with Al_2O_3 in the slag, which

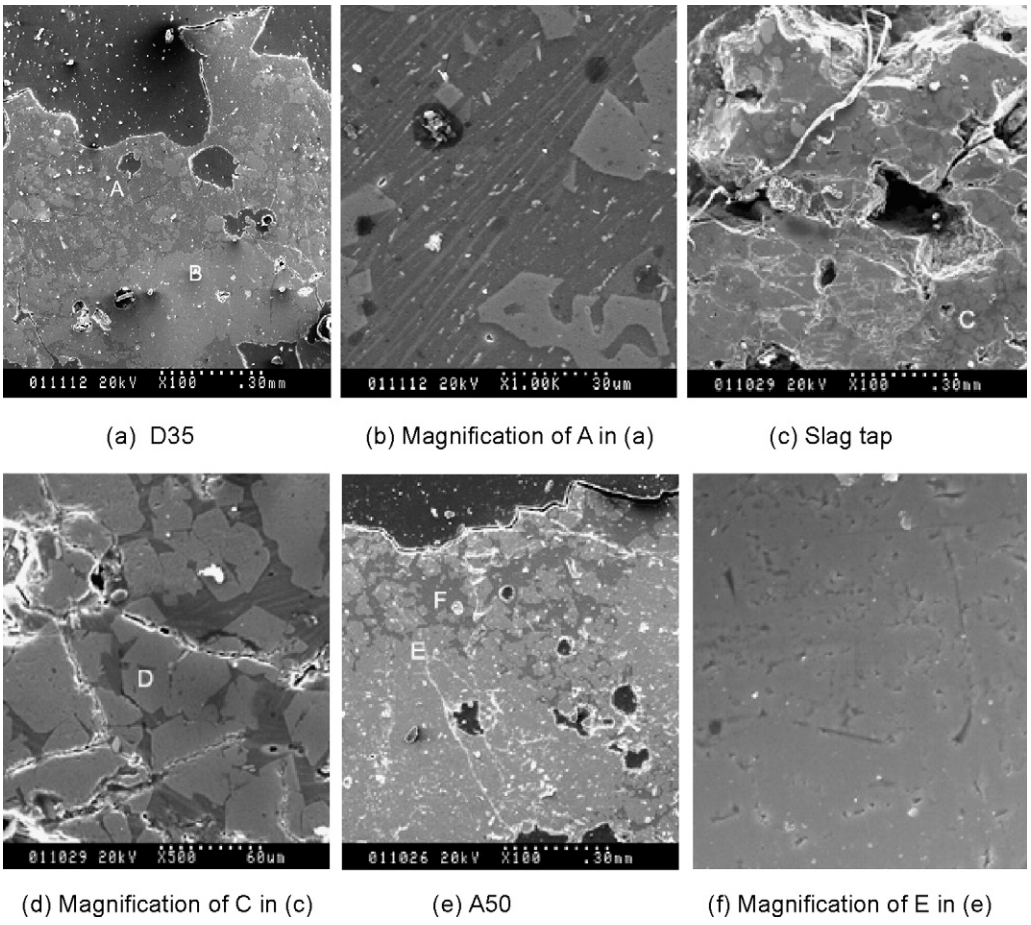

Fig. 7. SEM micrographs of slag face of D35 (a) and (b), slag tap (c) and (d), and A50 (e) and (f) samples from the IEA pilot scale gasifier.

occurs as Al_2O_3 in the slag diffuses into Cr_2O_3 from the edges. Again, the large, well-densified phase is less affected by slag, confirming that the refractory interaction with the infiltrating slag is a function of particle size, slag chemistry, and degree of densification.

Fig. 8(d) shows the region 9–10 mm from the slag face at a magnification of 1000×, and shows the corroded structures which are very similar to those in Fig. 8(b): Al-rich $(Cr,Al)_2O_3$ fragments (C), the large Cr-rich $(Cr,Al)_2O_3$ particles with a boundary layer (D), and the background $CaO–Al_2O_3–SiO_2$ phase (E). Again, the boundary showed a higher Al_2O_3 concentration than the center, and the concentration of Al_2O_3 decreased as the grey became lighter towards the center.

As in the laboratory tests, ZrO_2 does not seem to be greatly affected by slag corrosion even though it dissolves into the slag. ZrO_2 in a relatively corrosion resistant area did not show any evidence of physical change as shown in Fig. 9(a), but ZrO_2 in the severely degraded area showed that the smooth curved boundary became broken or extremely wavy (Fig. 9(b) and (c)), while its chemical composition showed no change [4].

The interaction of chromia refractory with FeO has been reported in the literature. Rawers et al. [5] investigated the corrosion of 75–25% $Cr_2O_3–Al_2O_3$ refractory, and reported $(Fe,Cr)_3O_4$, in the area near the slag/refractory interface. They also cited five references, which reported the formation of spinel phase in the same type of refractory. Even in the case of Al_2O_3 refractory with Cr_2O_3 as a minor component, the formation of Cr spinel phase was reported [6]. Guo et al. [7,8] reported the formation of $(Cr,Al,Fe)_2O_3$ from the analysis of microstructures. Thermodynamic equilibrium calculations by Pelton [9] predicted the formation of chromite when 0.2–5 g of 75–25% $Cr_2O_3–Al_2O_3$ refractory interacted with 100 g coal slag which contained 45% SiO_2, 24.5% Al_2O_3, 18.9% CaO, and 4% Fe_2O_3 at 1400 °C.

Unlike the formation of chromites described above, the change in Cr_2O_3 caused by Al_2O_3 in the slag has not been reported in the literature, except in the equilibrium study by Pelton [9]. Pelton predicted the formation of a $Cr_2O_3–Al_2O_3$ solid solution for the case described above. Rawer at al. [5] reported the formation of low-temperature melting $Ca(CrO_2)_2$, when a synthetic slag of 50% SiO_2 and 50% CaO was used. They stated that CaO could be a component, which could play an important role in refractory corrosion. With the slag which had about 6% CaO, we did not find any evidence to support the formation of $Ca(CrO_2)_2$ in the SEM/EDX measurements.

3.4. Crystalline phase analysis by XRD

From each laboratory corrosion test, one slag and three refractory samples were taken. The refractory samples were cut at 1 cm depth starting at the slag/refractory interface, and the crystalline phases were determined as a function of depth from

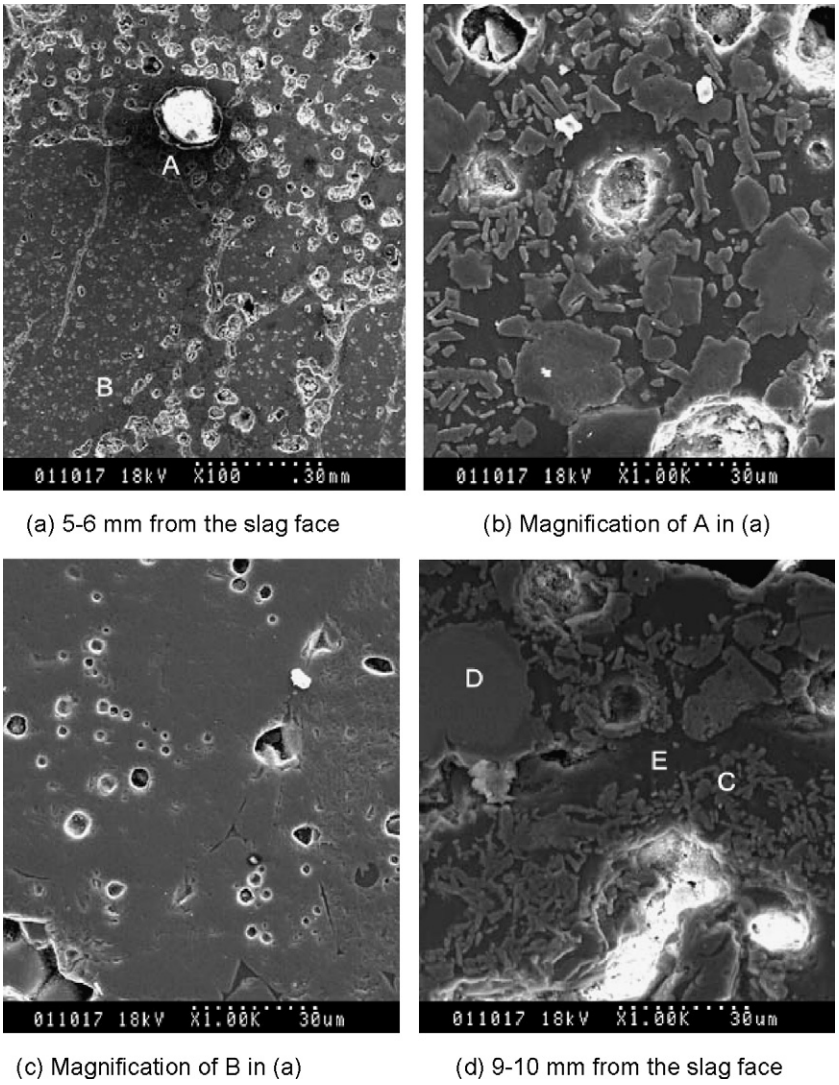

Fig. 8. SEM micrographs of B40 from the IEA pilot scale gasifier, 5–10 mm from the slag face: (a) 5–6 mm from the slag face, (b) magnification of A in (a), magnification of B in (a), and (d) 9–10 mm from the slag face at 1000×.

the interface. The XRD patterns of four samples from the 1500 °C experiment are shown in Fig. 10. For Datong ash slag, which contained the dendritic phase and dispersed Cr–Fe oxide as shown in Fig. 4(a)–(c), the XRD spectrum identified a spinel phase, either magnetite (Fe_3O_4) or chromite ($FeCr_2O_4$), as shown in Fig. 9(a). The XRD patterns of magnetite (Fe_3O_4) and chromite ($FeCr_2O_4$) were very similar. Therefore, the chemical composition of Fe–Cr oxides with various ratio of Fe/Cr can be

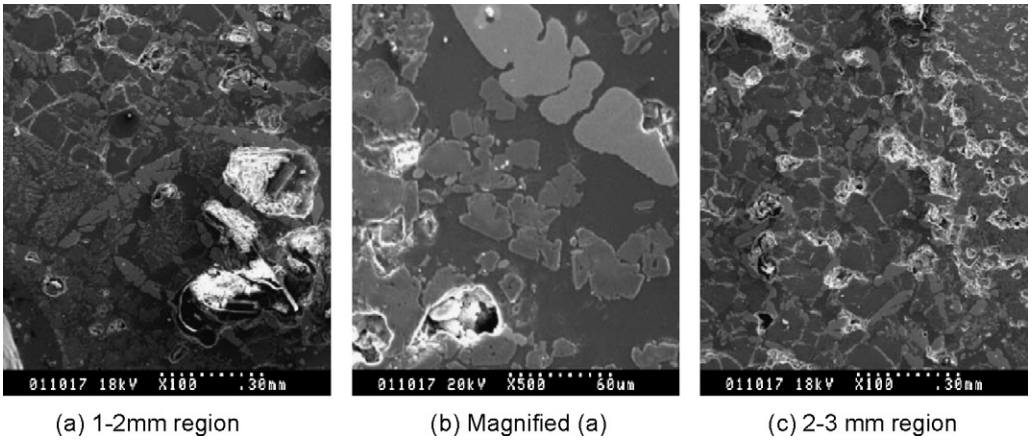

Fig. 9. SEM micrographs of ZrO_2 containing areas.

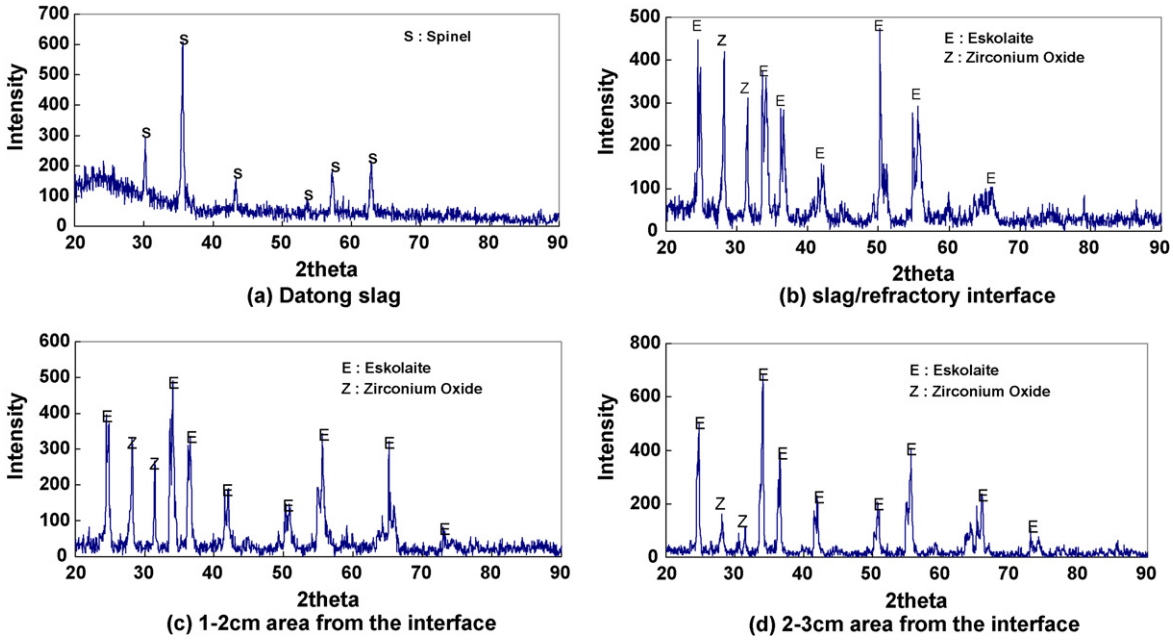

Fig. 10. XRD patterns of slag and refractory zones from 1500 °C slag exposure under a 20/80 mix of CO/CO_2 atmosphere: (a) Datong slag, (b) slag/refractory interface, (c) 1–2 cm from the interface, and (d) 2–3 cm from the interface.

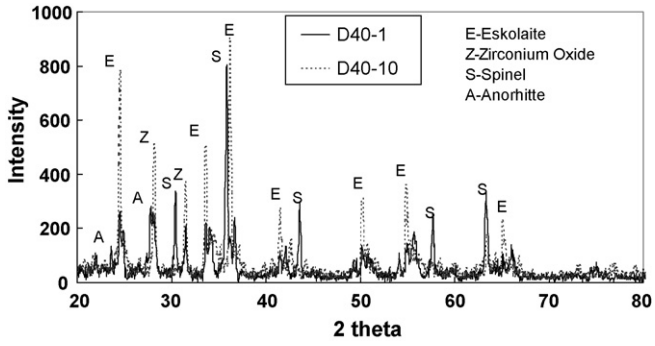

Fig. 11. XRD pattern of D40 from the IEA pilot scale gasifier at the slag/refractory interface and at a 10 cm depth from the interface.

expressed as $(Fe,Cr)_3O_4$. The XRD pattern of the three refractory samples in Fig. 9(b)–(d) were similar in peak positions, all showing the peaks of eskolaite (Cr_2O_3) and baddeleyite (ZrO_2), but the relative peak intensity varied due to heterogeneity of the sample. It was difficult to find the peaks for interaction products because $(Fe,Cr)_3O_4$ was found in only a 1 mm region from the refractory/slag interface.

Because of the much thicker layer of $(Fe,Cr)_3O_4$ on the spent refractory from a gasifier, the XRD pattern of the slag/refractory interface was able to determine more detailed changes in crystalline structure as shown in Fig. 11. Fig. 11 compares the XRD pattern of D40-1 (slag/refractory interface) with D40-10, the sample from the 10 cm depth, which is beyond the slag penetration depth. Chromite and anorthites ($CaAl_2Si_2O_8$) were identified in the D40-1 sample, while D40-10 contains only the refractory crystalline phases. All other slag face samples showed strong peaks of spinel phase and weak peaks of the anorthite phase. Anorthite is the crystalline phase commonly observed in coal slag. As the depth increased, the refractory phases such as eskolaite (Cr_2O_3) and baddeleyite (ZrO_2) became dominant.

3.5. Composition analysis of spent refractory from a gasifier by XRF

The depletion of Fe in the penetrating slag was also seen in the XRF composition analysis. Each spent refractory sample was cut into 1 cm sections from the refractory/slag interface

Table 3
Composition change in A50 sample as a function of depth

Depth	SiO_2	Al_2O_3	Fe_2O_3	CaO	Cr_2O_3	ZrO_2	MgO	MnO	Na_2O	K_2O	TiO_2
0–1 cm	13.3	21.6	4.5	3.6	44.4	9.2	1.5	0.07	1.04	0.21	0.69
1–2 cm	12.3	23.9	1.0	2.8	46.5	10.7	0.4	0.06	1.44	0.18	0.85
2–3 cm	13.8	27.0	1.	3.4	38.2	13.8	0.5	0.06	1.52	0.08	0.70
3–4 cm	10.4	23.4	0.8	2.7	50.9	9.4	0.3	0.05	1.07	0.04	0.88
4–5 cm	8.8	26.0	0.8	2.3	48.4	11.4	0.3	0.05	1.13	0.03	0.80
5–6 cm	7.8	24.0	0.7	2.2	53.2	10.0	0.30	0.05	0.75	0.03	0.92
Unused	8.3	24.6	0.72	1.8	52.7	9.4	0.3	0.07	1.00	0.03	1.00

and roughly 1 g of each section was used in the XRF composition analysis. The results for A50 are given in Table 3, and show that the Fe_2O_3 concentration rapidly decreased from 4.51% at the 0–1 cm layer to 1.02% in the next sample, and remained at less than 1%, which is the level of Fe_2O_3 in the raw brick, in all samples beyond 2 cm depth. The concentrations of SiO_2 also decreased as the depth increased: SiO_2 decreased from about 13% on the surface to the level in the raw refractory after the 4 cm of depth, and the CaO concentration was in the 2.8–3.6% range up to 3 cm depth, and then decreased.

The XRF composition data supports the conclusions from the microphase analyses by SEM/EDX; in the interaction of a chromia refractory with coal slag, FeO in the slag reacts first with Cr_2O_3 in the refractory until there is no FeO left in the penetrating slag.

4. Conclusions

The chemical interaction of chromia refractory with a coal slag occurred via a reaction between Cr_2O_3 in the refractory and FeO and Al_2O_3 in the slag. FeO reacted with Cr_2O_3 at the slag/refractory interface and formed $FeCr_2O_4$. After all FeO was depleted, Al_2O_3 in the infiltrating slag diffused into the Cr_2O_3 grain, forming $(Al,Cr)_2O_3$ on the outer edges of the particle. The corrosion resistance of Cr_2O_3 varied with the particle size and the extent of densification, and higher resistance was observed in the larger and more densified particles. There was no chemical change in ZrO_2, but it may have dissolved in the slag. The composition analyses and the crystalline phase analyses also support chromite formation at the interface, and subsequent depletion of Fe. When the exposure temperature and time were varied, the percent slag penetrated increased with the exposure time and temperature, but the changes in microstructures were difficult to quantify.

Acknowledgements

We gratefully acknowledge the Institute of Advance Engineering for providing spent samples and refractory powders. This research was supported by the Korean Ministry of Commerce, Industry and Resources via Project 2000-N-CO02-P-01, ‘‘Technology Demonstration for the Integrated Gasification System and the Development of Related Simulation Technologies,’’ and Hong-Ik University Research Fund, 2004.

References

[1] J. Rawers, L. Iverson, K. Collins, Initial stages of coal slag interaction with high chromia sesquioxide refractories, J. Mater. Sci. 37 (2002) 531–538.
[2] C. Dogan, K.-S. Kwong, J. Bennett, R. Chinn, C. Dahlin, Improved refractories for IGCC systems, http://www.industrialheatingcom/CDA/Articleinformation/Features/BN 4337-07-15 (Posted on September 2002).
[3] KS L 3130, Testing Method for Slag Corrosion of Refractories using Crucibles (revised on August 1996).
[4] H.B. Kim, MS Thesis, Hongik University, Seoul, Korea, 2002.
[5] J. Rawers, K. Collins, Rawer, M. Peck, Oxides reactions with a high-chrome sesquioxide refractory, J. Mater. Sci. 36 (2001) 4837–4843.
[6] C.-F. Chan, Y.-C. Ko, Effect of Cr_2O_3 on slag resistance of Al_2O_3–SiO_2 refractories, J. Am. Ceram. Soc. 75 (10) (1992) 2857–2861.
[7] Z.-Q. Guo, H. Zhang, The optimization of the microstructure and phase assemblage of high chromia refractories, J. Eur. Ceram. Soc. 19 (1999) 113–117.
[8] Z.-Q. Guo, B.-O. Hah, H. Dong, Effect of coal slag on the wear rate and microstructure of the ZrO_2-bearing chromia refractories, Ceram. Int. 23 (1997) 489–496.
[9] A.D. Pelton, thermodynamic databases and equilibrium calculations in metallurgical processes, Pure Appl. Chem. 69 (5) (1997) 969–978.